

Phase field modelling and simulation of damage occurring in human vertebra after screws fixation procedure

Deison Preve^a, Pietro Lenarda^{b,*}, Daniele Bianchi^c, Alessio Gizzi^c

^a

^bIMT School for Advanced Studies Lucca, Piazza San Francesco 19, 55100 Lucca, Italy

^cDepartment of Engineering, University of Rome Campus Bio-Medico, 00128 Rome, Italy

Abstract

The present endeavor numerically exploits the use of a phase-field model to simulate and investigate fracture patterns, deformation mechanisms, damage, and mechanical responses in a human vertebra after the incision of pedicle screws under compressive regimes. Moreover, the proposed phase field framework can elucidate scenarios where different damage patterns, such as crack nucleation sites and crack trajectories, play a role after the spine fusion procedure, considering several simulated physiological movements of the vertebral body. A convergence analysis has been conducted for the vertebra-screws model, considering several mesh refinements, which has demonstrated good agreement with the existing literature on this topic. Consequently, by assuming different angles for the insertion of the pedicle screws and taking into account a few vertebral motion loading regimes, a plethora of numerical results characterizing the damage occurring within the vertebral model has been derived. Overall, the phase field results may shed more light on the medical community, which will be useful in enhancing clinical interventions and reducing post-surgery bone failure and screw loosening.

Keywords: Phase field approach to fracture; Human Vertebra; Pedicle Screws Fixation; Numerical-experimental comparison.

1. Introduction

Originated from mathematical techniques based on Γ -convergence [1, 2] and tailored for the approximation of free discontinuity problems [3, 4], the phase field regularization of brittle fracture proposed by Francfort and Marigo [5] has attracted a remarkable attention within the computational fracture mechanics community over the last decade. As compared to other computational methods for damage and fracture simulation in materials and components, such as for instance the Crack Band Model [6], the Smeared Crack Model [7], non-local and diffuse damage models [8, 9], or gradient damage models [10], the phase field approach offers an elegant solution for problems involving linear elastic fracture mechanics. This solution is pursued through an energy minimization

*Corresponding author. Tel: , e-mail: pietro.lenarda@imtlucca.it

which, in the Γ -convergence limit, consistently reproduces the Griffith theory of fracture. The phase field approach to fracture, further analysed in [11, 12], has been applied in a considerable series of works proposing comparisons with other non-local damage models and discussing several detailed aspects regarding the finite element implementation [13–19]. In this context, it is worth recalling the fundamental contribution by Miehe and co-workers [20, 21] that were the first to propose a robust finite element implementation of the phase field for brittle fracture, specialized to account for damage irreversibility and based on a suitable degradation mechanism able to simulate situations involving tensile stress states.

The state-of-the-art literature on phase field models clearly shows that the approach is mature for technical applications. In this regards, Tannè et al. [22] have recently assessed the capabilities of the phase field approach (see in particular the AT1 and the AT2 models) to predict crack nucleation from V-notches and from points with stress concentrations. Phase field modeling has numerous applications, especially in the field of biomedical engineering, particularly in the study of bone fractures. In this regard, fractures in the vertebrae can be challenging to analyze and treat due to their complex shapes and locations [23]. However, phase field modeling can help by simulating the fracture process and shedding light on the underlying mechanisms involved. In particular, phase field modeling can be used to investigate the impact of vertebral fixation and screw placement on the healing of vertebral fractures. By incorporating the presence of screws and other fixation devices into the simulation, researchers can evaluate the mechanical stability of the fracture site and predict the potential for screw loosening or failure. Additionally, researchers can gain insights into the effects of different placement strategies on the fracture propagation process.

Quantitative and qualitative finite element models are being developed to evaluate damage patterns and predict crack propagation in biological tissues. So much so, recently, the capability of a plethora of phase field implementations for modelling and analysing crack growth in bone tissue has been successfully applied [24], thus phase field theory seems a promissory approach to assess bone fracture patterns. In this context, the biomechanical problem of characterizing damage and predicting crack trajectories in a human vertebra after the fixation procedure of pedicle screws (see Fig. 1(a)) can be tackled utilizing a phase field method.

Metallic pedicle screws are used in spine fusion procedures when the intervertebral discs were damaged by aging or any trauma, causing the vertebrae to rub against each other and compress the nerves that pass through them. Spinal fusion joins two or more diseased vertebrae together, preventing motion at the vertebral segment [25]. The screws are inserted into the respective pedicle regions, connecting the screws through a vertical rod, providing a means for gripping onto a vertebral segment and limiting its motion, resulting in stable spine fixation. Bone damage and screw loosening may occur due to various post-operative events [26]. Furthermore, the mechanical behavior of the pedicle screw insertion angle has been experimentally investigated [27, 28]. Nonetheless, finite element analysis allows for the assessment of numerous possible failure scenarios that may occur after the surgical procedure requiring screw insertion, as well as the character-

ization of fracture damage and estimation of mechanical responses under varying screws fixation angles [29]. Thereby, the impact of screw configuration angular parameters in fracture pattern and stress distributions were investigated via computational model considering a stress-based criterion [30, 31]. In the study by [23], the mechanical behaviour of instrumented metastatic vertebra in presence of pedicle screws was investigated. The findings showed that the prediction of mechanical properties was affected by the size and location of the metastasis. It was also concluded that a metastasis situated near the screws produces a higher fracture load response compared to a metastasis far from the screws. As a consequence, a finite element phase field model is hereof implemented in order to validate numerically the existing outcomes in the literature resulting from the variation of the screws insertion angle in a human vertebra, with the aim of further developing a coupled model with two or more fused vertebrae.

The paper is organized as follows: Section 2 provides the CAD models of the screws and the vertebra, which are discretized and have their material properties set. It also covers the virtual insertion of pedicle screws into the vertebra. Section 3 introduces the phase field finite element method strategy implemented in this study. The staggered and monolithic phase field models are detailed in Section 4. Section 5 presents the boundary conditions and parameter setup for the numerical phase field method. Additionally, it includes a mesh sensitivity analysis of the phase field framework applied to several discretized models of vertebra-screws. Finally, Section 6 presents the main results in terms of damage patterns. It considers various screws insertion trajectories for different vertebral movements and includes a discussion comparing the outcomes with other relevant works in this field.

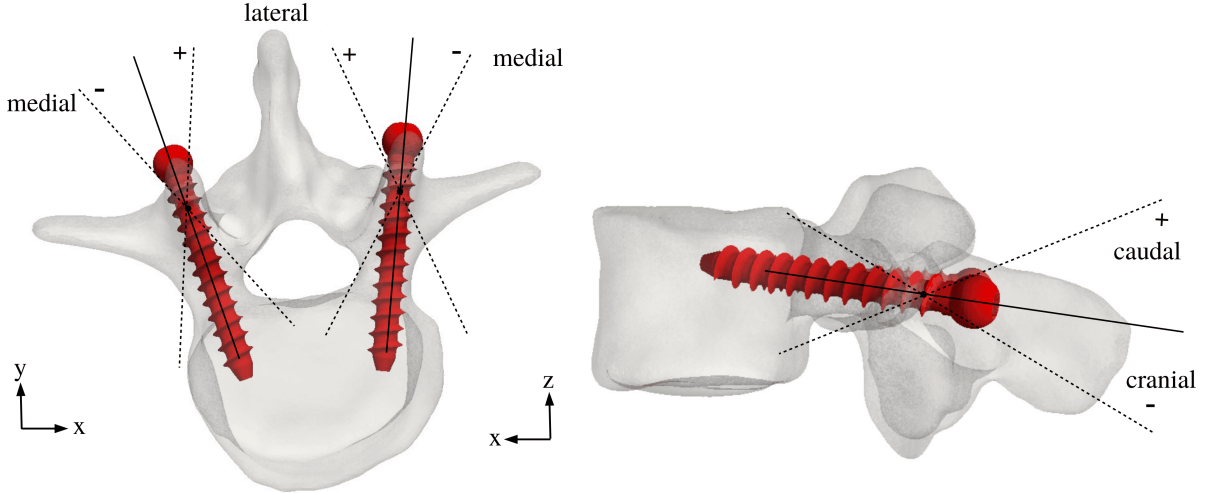
2. Human vertebra-pedicle screws finite element model

2.1. Models and materials

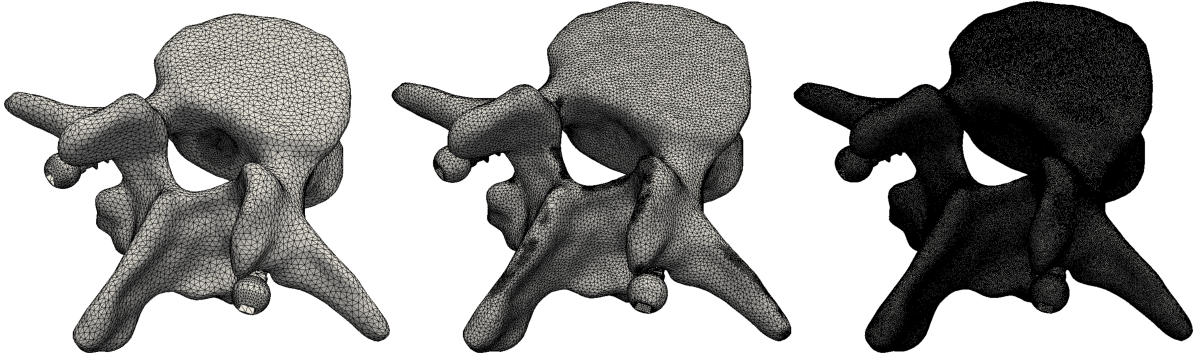
The L4 lumbar vertebra model was obtained from a Computer Tomography (CT) scan images from the spine of 49-year-old female patient, as described in [25]. The solid cylindrical pedicle screws have length of 40 mm. The major and minor diameters of screws are 6.5 mm and 4.3 mm, respectively (please see [25, 29] for additional details). The CAD models of the pedicle screws virtually inserted in the L4 vertebra are depicted in Fig. 1. The phase field model has been evaluated for three different screws fixation paths, indicated by the vector $\vec{\alpha} = (\alpha_1, \alpha_2)$. Here, α_1 represents the insertion angle in the cranio-caudal (CC) direction, and α_2 indicates the insertion angle in the medio-lateral (ML) direction [25], as shown in Fig. 1(a). In particular, the mesh sensitivity analysis is conducted using the screws insertion trajectory combination $\vec{\alpha} = (-5, 0)$, which means that the screws are fixed with a negative angle of -5° in the CC direction and a neutral angle of 0° in the ML direction.

To import the combined vertebra-screws CAD model into the finite element environment FEniCS [32], uniform tetrahedral meshes are constructed. This is achieved by transferring the assembled STL model's triangular mesh into the pre-processing software HyperMesh [33], which generates the required tetrahedral solid. The solid is then

assessed and converted into a MSH file using the Gmsh platform [34]. Multiple refined meshes have been created, ranging from 60 thousand elements to 700 thousand elements. Please refer to Fig. 1(b) for visualization of these meshes.



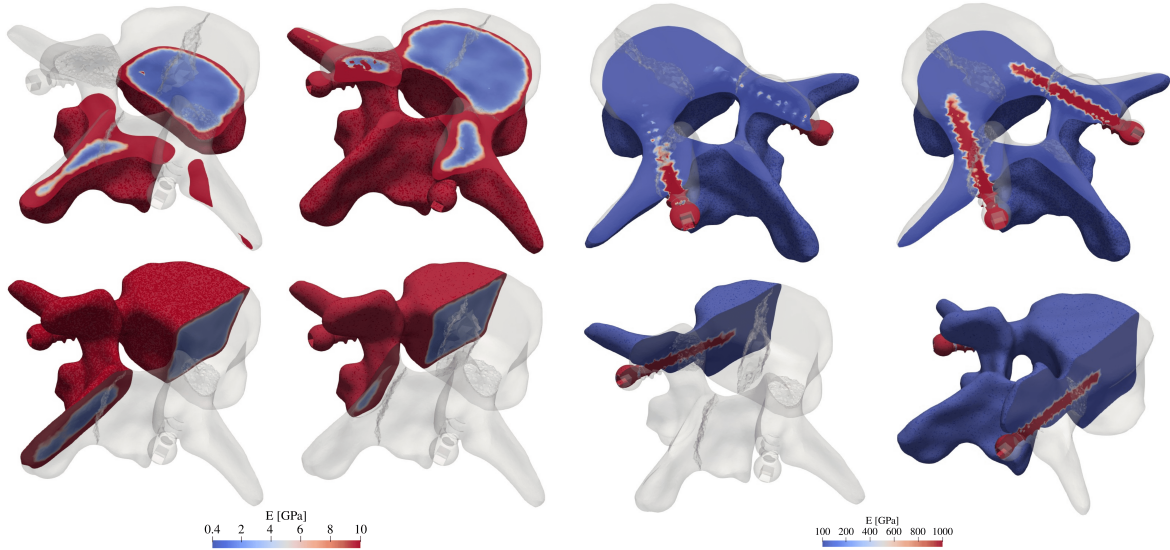
(a) Identification of CC and ML directions of the pedicle screws virtually inserted.



(b) Uniform computational discretized vertebra-screws meshes. From left to right: 100 DoF, 350 DoF, 700 DoF.

Fig. 1: CAD-based finite element of the vertebra-screws model.

Bone density properties have been considered for the material of the L4 vertebra using CT data [35–37]. In this regard, a constant Poisson’s ratio of $\nu = 0.3$ was assumed, and isotropic and linear elastic material properties were adopted with a heterogeneous distribution of the Young’s modulus E . This distribution differentiates the cortical bone from the trabecular bone. For more details, please refer to [25, 29]. For trabecular bone, an elastic modulus ranging between 0 and 3 GPa was derived, while for cortical bone, the range was between 12 and 14 GPa, as shown in Fig. 2(a). In what regards to the pedicle screws, surgical procedures commonly use biomedical implants or replacements made of the titanium alloy Ti-6Al-4V [38–40]. Therefore, the chosen mechanical properties for the pedicle screws are a Young’s modulus of 110 GPa and a Poisson’s ratio of 0.4.



(a) Young's modulus (GPa) distribution of the vertebra. The red color represents the high stiffness layer given by the cortical bone, while the blue color indicates low stiffness layer given by the trabecular bone. (b) Young's modulus (GPa) distribution of the pedicle screws. The red color illustrates the high stiffness assumed for the pedicle screws.

Fig. 2: Interpolated Young's modulus (GPa) distribution of the model vertebra-screws. correct stiffness values.

3. Phase-field approaches to fracture with spectral decomposition

With reference to an arbitrary body occupying a domain $\Omega \in \mathbb{R}^{n_{dim}}$, with boundary $\partial\Omega \in \mathbb{R}^{n_{dim}-1}$, in the Euclidean space of dimension n_{dim} , in which an evolving internal discontinuity Γ is postulated to exist, a material point is denoted by \mathbf{x} and body forces by $\mathbf{b} : \Omega \rightarrow \mathbb{R}^{n_{dim}}$. Mixed conditions are prescribed along non-overlapping Neumann and Dirichlet regions of the boundary $\partial\Omega_N \cup \partial\Omega_D = \partial\Omega$ in the usual form

$$\mathbf{u} = \bar{\mathbf{u}} \text{ on } \partial\Omega_D \text{ and } \boldsymbol{\sigma} \cdot \mathbf{n} = \bar{\mathbf{T}} \text{ on } \partial\Omega_N, \quad (1)$$

where \mathbf{n} denotes the outward unit normal to the boundary, \mathbf{u} is the displacement field and $\boldsymbol{\sigma}$ is the Cauchy stress tensor, while $\bar{\mathbf{u}}$ and $\bar{\mathbf{T}}$ are prescribed surface displacements and tractions.

The variational approach to brittle fracture, governing crack nucleation, propagation and branching, is set up through the definition of the free energy functional [20],

$$\Pi(\mathbf{u}, \Gamma) = \Pi_\Omega(\mathbf{u}, \Gamma) + \Pi_\Gamma(\Gamma), \quad (2)$$

embodying an additive decomposition between the elastic bulk energy Π_Ω stored in the damaged body and the energy Π_Γ necessary to nucleate and propagate a Griffith crack [41], defined as

$$\Pi_\Omega(\mathbf{u}, \Gamma) + \Pi_\Gamma(\Gamma) = \int_{\Omega \setminus \Gamma} \psi^e(\boldsymbol{\varepsilon}) \, d\mathbf{x} + \int_\Gamma \mathcal{G}_c(\mathbf{u}, s) \, d\mathbf{x}, \quad (3)$$

where ψ^e is the elastic strain energy density, function of strain $\boldsymbol{\varepsilon}$, and \mathcal{G}_c is the fracture energy, function of the displacement \mathbf{u} and of the phase field variable s . The latter parameter $s \in [0, 1]$ is an internal state variable, ranging between 0 and 1 and representing isotropic damage, so that $s = 0$ is representative of the intact material, while $s = 1$ characterizes the fully damaged state.

3.1. The regularized variational formulation

Within the regularized framework of the phase field approach [12, 20, 42, 43], the potential energy of the system can be decomposed into two terms as following

$$\Pi(\mathbf{u}, s) = \int_{\Omega} \psi^e(\boldsymbol{\varepsilon}, s) \, d\mathbf{x} + \mathcal{G}_c \int_{\Omega} \gamma(s, \nabla s) \, d\mathbf{x} , \quad (4)$$

where $\psi^e(\boldsymbol{\varepsilon}, s)$ is the energy density of the bulk, now function of the damaged parameter s , and $\gamma(s, \nabla s)$ is the crack density functional, with ∇ denoting the spatial gradient operator. As a result, the total free energy density of the bulk $\hat{\psi}$ reads as

$$\hat{\psi}(\boldsymbol{\varepsilon}, s) = \psi^e(\boldsymbol{\varepsilon}, s) + \mathcal{G}_c \gamma(s, \nabla s).$$

The functional $\gamma(s, \nabla s)$ is assumed to be a convex function of s and its gradient ∇s and can be written, in agreement with the following expressions characterizing the AT2 model, respectively, as:

$$\gamma(s, \nabla s) = \frac{1}{2} \left(\frac{s^2}{l} + l |\nabla s|^2 \right), \quad (5)$$

where l_0 stands for a regularisation characteristic length that can be related to the Young's modulus, the fracture toughness, and the tensile strength of the material, as specified in Section 5.

To avoid the development of damage in compression, so to allow fracture growth only under tensile stress states, the following 'tensile/compressive' decomposition is herein assumed for the energy density in the bulk $\psi^e(\boldsymbol{\varepsilon}, s)$ [20, 44–47] and included in the formulation:

$$\psi^e(\boldsymbol{\varepsilon}, s) = g(s) \psi_+^e(\boldsymbol{\varepsilon}) + \psi_-^e(\boldsymbol{\varepsilon}), \quad (6)$$

where $g(s)$ is a damage function that is assumed in the simple form $g(s) = (1 - s)^2 + k$, where k is a residual stiffness (introduced to avoid ill-conditioning) and the positive and negative parts of the energy density are defined as

$$\psi_{\pm}^e(\boldsymbol{\varepsilon}) = \frac{\lambda}{2} (\text{tr} \boldsymbol{\varepsilon}_{\pm})^2 + \mu \text{tr} (\boldsymbol{\varepsilon}_{\pm}^2), \quad (7)$$

where λ and μ are the Lamé constants, $\text{tr}(\cdot)$ denotes the trace operator and the positive and negative parts of the strain $\boldsymbol{\varepsilon}_{\pm}$ are defined as follows. With reference to the spectral

representation for the strain (with eigenvalues ϵ_i and unit eigenvectors \mathbf{e}_i), denoted as

$$\boldsymbol{\varepsilon} = \sum_{i=1}^3 \epsilon_i \mathbf{e}_i \otimes \mathbf{e}_i, \quad (8)$$

the strain is additively decomposed as $\boldsymbol{\varepsilon} = \boldsymbol{\varepsilon}_+ + \boldsymbol{\varepsilon}_-$, so that the tensile and compressive parts associated to $\boldsymbol{\varepsilon}$ are

$$\boldsymbol{\varepsilon}_+ = \sum_{i=1}^3 \langle \epsilon_i \rangle \mathbf{e}_i \otimes \mathbf{e}_i, \quad \text{and} \quad \boldsymbol{\varepsilon}_- = - \sum_{i=1}^3 \langle -\epsilon_i \rangle \mathbf{e}_i \otimes \mathbf{e}_i, \quad (9)$$

respectively, where the Macaulay bracket operator is defined for every scalar x as $\langle x \rangle = (x + |x|)/2$.

A standard derivation [48] leads Eq. (7) to the Cauchy stress tensor from the strain energy density:

$$\boldsymbol{\sigma} = g(s)\boldsymbol{\sigma}_+ + \boldsymbol{\sigma}_- = \{(1-s)^2 + k\} (\lambda \text{tr} \boldsymbol{\varepsilon}_+ \mathbf{I} + 2\mu \boldsymbol{\varepsilon}_+) + \lambda \text{tr} \boldsymbol{\varepsilon}_- \mathbf{I} + 2\mu \boldsymbol{\varepsilon}_-, \quad (10)$$

where \mathbf{I} denotes the second-order identity tensor. The thermodynamic consistency of the above constitutive theory, in agreement with the Clausius-Duhem inequality, has been addressed in [20].

3.2. Weak form of the variational problem

The weak form corresponding to the phase field model for brittle fracture can be derived following a standard Galerkin procedure. In particular, the weak form of the coupled displacement and phase field damage problem according to Eq. (4) is:

$$\delta \Pi = \int_{\Omega} \boldsymbol{\sigma}(\mathbf{u}) : \boldsymbol{\varepsilon}(\mathbf{v}) \, d\mathbf{x} - \int_{\Omega} 2\psi_+^e(\boldsymbol{\varepsilon})(1-s)\phi \, d\mathbf{x} + \int_{\Omega} \mathcal{G}_c \left\{ \frac{1}{l} s\phi + l \nabla s \cdot \nabla \phi \right\} \, d\mathbf{x} + \delta \Pi_{\text{ext}}, \quad (11)$$

where \mathbf{v} is the vector of the displacement test functions defined on $\mathbf{H}_0^1(\Omega)$, ϕ stands for the phase field test function defined on $H_0^1(\Omega)$. Eq. (11) holds for every test functions \mathbf{v} and ϕ . The external contribution to the variation of the bulk functional in Eq. (11) is defined as follows:

$$\delta \Pi_{\text{ext}}(\mathbf{u}, \mathbf{v}) = \int_{\partial\Omega} \bar{\mathbf{T}} \cdot \mathbf{v} \, d\Gamma + \int_{\Omega} \mathbf{b} \cdot \mathbf{v} \, d\mathbf{x}. \quad (12)$$

4. Numerical FE schemes

4.1. Staggered solution scheme

The mechanical problem can be stated as: given the prescribed loading condition $\bar{\mathbf{u}}_n$ and $\bar{\mathbf{T}}_n$ at step n , find $\mathbf{u} \in \mathbf{U} = \{\mathbf{u} \mid \mathbf{u} = \bar{\mathbf{u}}_n \text{ on } \partial\Omega_u, \mathbf{u} \in \mathbf{H}^1(\Omega)\}$ such that

$$\mathcal{E}_{\mathbf{u}}(\mathbf{u}, s; \mathbf{v}) := \int_{\Omega} \boldsymbol{\sigma}(\mathbf{u}) : \boldsymbol{\varepsilon}(\mathbf{v}) \, d\mathbf{x} - \int_{\partial\Omega} \bar{\mathbf{T}}_n \cdot \mathbf{v} \, d\Gamma - \int_{\Omega} \mathbf{b} \cdot \mathbf{v} \, d\mathbf{x} = 0, \quad \forall \mathbf{v} \in \mathbf{H}_0^1(\Omega), \quad (13)$$

while the phase field problem is formulated as: find $s \in S = \{s \mid s = 1 \text{ on } \Gamma, s \in H^1(\Omega)\}$ such that $\forall \phi \in H_0^1(\Omega)$:

$$\mathcal{E}_s(\mathbf{u}, s; \phi) := \int_{\Omega} \mathcal{G}_c l \nabla s \cdot \nabla \phi \, d\mathbf{x} + \int_{\Omega} \left(\frac{\mathcal{G}_c}{l} + 2H \right) s \phi \, d\mathbf{x} - \int_{\Omega} 2H \phi \, d\mathbf{x} = 0, \quad (14)$$

where $H(\boldsymbol{\varepsilon}) = \max_{\tau \in [0, t]} \{\psi_+^e(\boldsymbol{\varepsilon}(\tau))\}$ is the strain history function, accounting for the irreversibility of crack formation [17, 20].

To solve the quasi-static evolution problems for brittle fracture, isoparametric linear triangular finite elements are used for the spatial discretization, and a staggered solution scheme is considered. Staggered schemes based on alternate minimization exploit the convexity of the energy functional with respect to each individual variable \mathbf{u} and s [49]. Here, an *ad hoc* developed solver has been implemented in the software **FEniCS**, see Alg. 1 for the staggered algorithm description. A series of benchmark tests taken from [20, 50] has been carried out to validate the methodology.

4.2. Newton-Raphson procedure

Even if the mechanical problem has been split into Eqs. (13) and (14), so that the phase field is reduced to a linear problem, nonlinearity still remains, because of the piece-wise linearity of the constitutive law, which includes a spectral decomposition of the strain. Therefore, a consistent linearization is required, so that the linear form defined by the residual can be written as:

$$F_{\mathbf{u}}(\mathbf{u}, s; \mathbf{v}) = \int_{\Omega} \left\{ ((1-s)^2 + k) \boldsymbol{\sigma}_+(\mathbf{u}) : \boldsymbol{\varepsilon}(\mathbf{v}) + \boldsymbol{\sigma}_-(\mathbf{u}) : \boldsymbol{\varepsilon}(\mathbf{v}) \right\} d\mathbf{x} + \int_{\partial\Omega} \bar{\mathbf{T}} \cdot \mathbf{v} \, d\Gamma - \int_{\Omega} \mathbf{b} \cdot \mathbf{v} \, d\mathbf{x}. \quad (15)$$

Given \mathbf{u}^k the current Newton-Raphson approximate solution at iteration k , the correction $\delta\mathbf{u}$ is therefore the solution of the following linear variational problem: find $\delta\mathbf{u} \in \mathbf{U}_0 = \{\mathbf{u} \mid \mathbf{u} = \mathbf{0} \text{ on } \partial\Omega_u, \mathbf{u} \in \mathbf{H}^1(\Omega)\}$ such that $J_{\mathbf{u}}(\delta\mathbf{u}, \mathbf{u}^k, s; \mathbf{v}) = -F_{\mathbf{u}}(\mathbf{u}^k, s; \mathbf{v})$, $\forall \mathbf{v} \in \mathbf{H}_0^1(\Omega)$, and then iterate as $\mathbf{u}^{k+1} = \mathbf{u}^k + \delta\mathbf{u}$. The Jacobian entering the formulation is

$$J_{\mathbf{u}}(\delta\mathbf{u}, \mathbf{u}, s; \mathbf{v}) = \int_{\Omega} \left\{ ((1-s)^2 + k) \partial\boldsymbol{\sigma}_+(\delta\mathbf{u}, \mathbf{u}) : \boldsymbol{\varepsilon}(\mathbf{v}) + \partial\boldsymbol{\sigma}_-(\delta\mathbf{u}, \mathbf{u}) : \boldsymbol{\varepsilon}(\mathbf{v}) \right\} d\mathbf{x}; \quad (16)$$

for details about the terms $\partial\boldsymbol{\sigma}_-$, $\partial\boldsymbol{\sigma}_+$, please see [18].

At this stage, it is fundamental to remark that, in order to predict crack trajectories in human vertebrae under tensile/compressive stress states, the phase field finite element method will be formulated. This formulation involves decomposing the strain energy density $\psi^e(\mathbf{u}, s)$ in Eq. (6) based on spectral diagonalization, as described in [20], into active and passive parts. This decomposition allows for the application of material response degradation only in tension. The variational formulation is then implemented

Algorithm 1 Staggered iterative scheme for phase field fracture at a step $n \geq 1$

- 1: **Input:** Displacements and phase field $(\mathbf{u}_{n-1}, s_{n-1})$ and prescribed loads $(\bar{\mathbf{u}}_n, \bar{\mathbf{T}}_n)$:
 - 2: Initialize $(\mathbf{u}^0, s^0) := (\mathbf{u}_{n-1}, s_{n-1})$;
 - 3: **for** $k \geq 1$ staggered iteration **do**:
 - 4: Given s^{k-1} , solve the mechanical problem (13): $\mathcal{E}_{\mathbf{u}}(\mathbf{u}, s^{k-1}; \mathbf{v}) = 0$ for \mathbf{u} , set $\mathbf{u} := \mathbf{u}^k$;
 - 5: Given \mathbf{u}^k , solve the phase field problem (14): $\mathcal{E}_s(\mathbf{u}^k, s; \phi) = 0$ for s , set $s := s^k$;
 - 6: **if** $\max\{\|\mathbf{u}^k - \mathbf{u}^{k-1}\|/\|\mathbf{u}^k\|, |s^k - s^{k-1}|/|s^k|\} < \text{tol}$: **then**
 - 7: set $(\mathbf{u}^k, s^k) := (\mathbf{u}_n, s_n)$;
 - 8: **else** $k + 1 \rightarrow k$.
 - 9: **end if**
 - 10: **end for**
 - 11: **Output:** (\mathbf{u}_n, s_n) .
-

in the FEniCS environment, utilizing the MPI (message passing interface) parallelization library, which accelerates the computational time.

4.3. Monolithic solution scheme

A monolithic solver has also been implemented in FEniCS. The tangent operator of the non-linear variational functional,

$$\begin{aligned} \mathcal{E}_{\mathbf{u},s}(\mathbf{u}, s; \mathbf{v}, \phi) := & \int_{\Omega} \boldsymbol{\sigma}(\mathbf{u}) : \boldsymbol{\varepsilon}(\mathbf{v}) \, d\mathbf{x} - \int_{\Omega} 2H(\boldsymbol{\varepsilon})(1-s)\phi \, d\mathbf{x} + \\ & \int_{\Omega} \mathcal{G}_c \left\{ \frac{1}{l} s \phi + l \nabla s \cdot \nabla \phi \right\} \, d\mathbf{x} + \int_{\partial\Omega} \bar{\mathbf{T}} \cdot \mathbf{v} \, d\Gamma + \int_{\Omega} \mathbf{b} \cdot \mathbf{v} \, d\mathbf{x}, \end{aligned} \quad (17)$$

is computed via the symbolic derivative `derivative`, the monolithic algorithm scheme can be visualized in Alg. 2.

Algorithm 2 Monolithic iterative scheme for phase field fracture at a step $n \geq 1$

- 1: **Input:** Displacements and phase field $(\mathbf{u}_{n-1}, s_{n-1})$ and prescribed loads $(\bar{\mathbf{u}}_n, \bar{\mathbf{T}}_n)$:
 - 2: Solve the coupled non-linear variational problem via Newton-Raphson iterative scheme:
 - 3: $\mathcal{E}_{\mathbf{u},s}(\mathbf{u}_n, s_n; \mathbf{v}, \phi) = 0, \quad \forall (\mathbf{v}, \phi) \in \mathbf{H}_0^1(\Omega) \times H_0^1(\Omega)$
 - 4: **Output:** (\mathbf{u}_n, s_n) .
-

5. Phase Field modelling to pedicle screws in human vertebra

5.1. Parameters calibration

The length scale l_0 parameter is deeply inserted for modelling phase field, considering that for a sufficiently small length scale l , the functional (11) converges to the total potential energy functional (2), in the sense that the global minimizers of Π_l will also

converge to that of Π . This entails that the length scale must be carefully chosen, rather than setting it arbitrarily. Having said that, on one hand, the characteristic length scale is related to the apparent material strength [51–53]. Particularly, once the base material properties are attributed, namely Young’s modulus E , critical energy release rate \mathcal{G}_c , then the characteristic length can be tuned as

$$l = \frac{27}{256} \left(\frac{\mathcal{G}_c E}{\sigma_{\max}^2} \right). \quad (18)$$

Consequently, the failure stress σ_{\max} was considered according to [25, 54, 55], so the length scale can be evaluated through Eq. (18).

On the other hand, the characteristic length scale can be interpreted, and therefore calibrated, as a structural factor. In particular, in a biological material, as cortical bone for instance, the length scale can be attributed to the lamellar microstructure, which may trap the crack tip within it, deflecting or stopping the leading edge of the crack [56]. Moreover, structural changes in cortical bone due to ageing affect crack path and damage properties [35, 57, 58].

In essence, the characteristic length scale that smears the regularized crack can be obtained either from microscopic structural-related mechanisms [59, 60], or from bone properties [61, 62]. As such, prior to determine the characteristic length scale through Eq. (18), a power-law equality is usually assumed by which the critical energy release rate \mathcal{G}_c is derived from bone density properties, namely

$$\mathcal{G}_c = \mathcal{G}_{c_0} \left(\frac{E}{E_0} \right)^\beta, \quad (19)$$

where the parameters have been set as $E_0 = 20.000$ MPa $\mathcal{G}_{c_0} = 0.01$ N/mm, and $\beta = 0.8$ are the base elastic modulus, the base critical energy release rate, the bone ash density and the power-law exponent, respectively. For those reasons, when a mesh sensitivity analysis is being conducted in a biological material, the phase field parameters must also be carefully examined and validated. As such, it has been performed in [24, 62], different values for the characteristic length scale have been considered, where the latter has calibrated phase field parameters after mechanical in-vitro experiments on human humeri bones. In addition, the critical energy release rate \mathcal{G}_c plays a crucial role in phase field modelling for bone application, where throughout experiments, different values of \mathcal{G}_c have been obtained at different aged cortical bones [57, 61]. Following these aspects, the critical energy release rate \mathcal{G}_c and the length scale have been calibrated using Eqs. (18) and 19, and validated from the experimental studies herein mentioned.

5.2. Boundary conditions, numerical implementation and mesh sensitivity analysis

Although spine models have been extensively exploited and validates in the literature [63], the present finite element phase field method focuses on a single vertebral body, as observed in other studies [29, 64]. In this study, the loadings are addressed on the inserted screws in the L4 vertebra, which will be simultaneously constrained. Throughout all the numerical implementations, the boundary conditions were set to

replicate the principal movements permitted by the vertebral column. For this purpose, the pedicle screws head have been loaded to reproduce flexion (bending forward) and extension (bending backwards) (green arrows in Fig. 3), rotation (torsion/twisting) (red arrows in Fig. 3). The centre of the L4 vertebra has been assumed as the rotation axis centre for the twisting loading mode. Meanwhile, a compressive force of $F_v = 5$ N has been applied to the superior endplate of the vertebral body, while the inferior endplate has been constrained. Furthermore, the vertebral fracture patterns have been simulated by incrementally applying a quasi-static force to the screw heads for all the studied movements. Fundamentally, the total force applied at each loading step corresponds to 10% of the constant compressive load F_v .

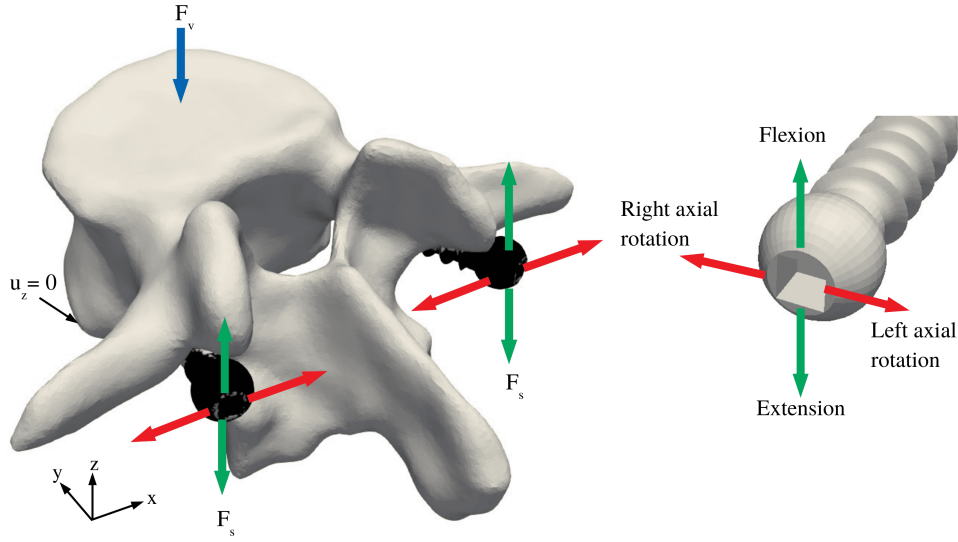
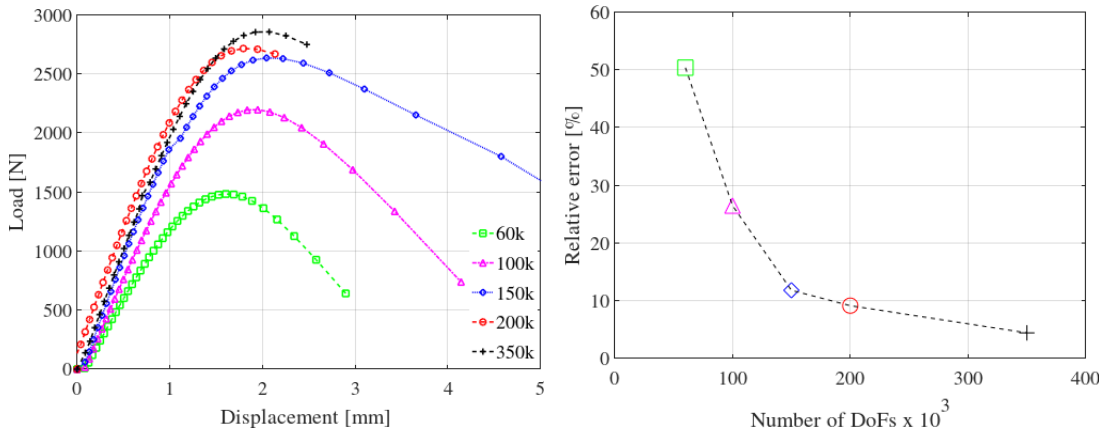


Fig. 3: Boundary conditions and loading regimes employed on the vertebra-screws models for numerical implementation.

The numerical phase field procedures were implemented in a High-Performance Computing (HPC) system, utilizing parallel computing and dividing the model into three smaller tasks. The computational time ranged from 2 hours for the coarsest mesh to 30 hours for the finest mesh. Six cores were utilized, with an average of 200 GB of RAM per core. It is worth mentioning that the extension and flexion loading modes required more time for simulation, necessitating the use of additional cores and computational memory to improve the efficiency of these movement modes.

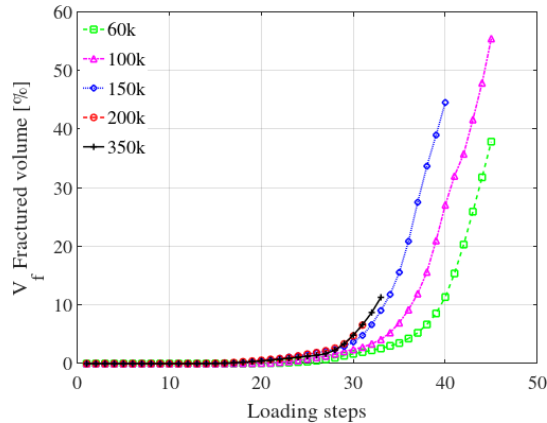
With the aim of achieving an appropriate mesh discretization for obtaining accurate numerical phase field responses for various physiological motions, a meticulous mesh sensitivity analysis has been conducted using the phase field finite element method. The vertebra-screws mesh model has been uniformly discretized at various refinements levels, ranging from 60.000 to 350.000. Fig. 4 presents the numerical analysis comparing the outcomes in the flexion loading mode for different mesh refinements, with the screws insertion angle set as $\vec{\alpha} = (-5, 0)$. Fig. 4(a) depicts the Load vs. Displacement curves juxtaposed, indicating that as the mesh becomes finer, the vertebra-screws model can

bear more load. Additionally, Fig. 4(b) illustrates the relative error as the number of elements increases. According to [25], it can be noticed that mesh convergence is satisfactorily achieved at a relative error of 5%. Therefore, assuming a mesh size between 200.000 and 350.00 elements is acceptable for characterizing the fracture patterns in the simulated physiological movements. Nonetheless, in terms of characterizing the damage patterns, the present mesh sensitivity analysis revealed no significant distinctions among the different mesh refinements. Moreover, the computational cost aligns well with the numerical outcomes using a mesh with 200.000 elements. This is further supported by Fig 4(c) which displays the fractured volume as the loading step varies. These convergence analyses demonstrate good agreement with previous studies [25, 29]. In terms of fracture type, although the phase field model captured similar damage patterns for all mesh refinements, coarser meshes exhibited more rapid fracture spread within the cortical part.



(a) Force vs. Displacement curves.

(b) Relative error as function of the number of degrees of freedom.



(c) Vertebral fractured volume as function of the loading steps.

Fig. 4: Mesh sensitivity analysis: Flexion mode movement at screws fixation angle of $\vec{\alpha} = (-5, 0)$.

In accordance with the estimations made in [62], an examination of the role played by the characteristic length scale l_0 is also developed here. Taking into consideration the

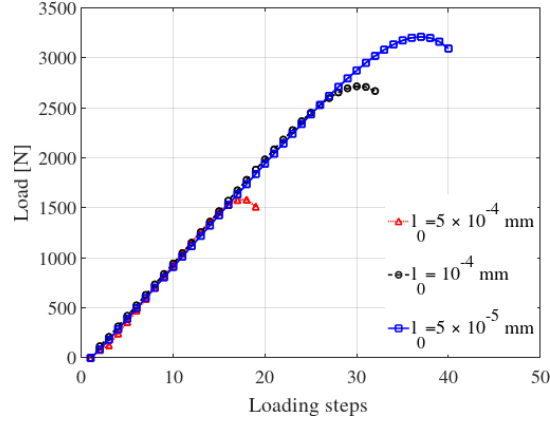


Fig. 5: Load vs. loading steps obtained for different values of the length scale parameter l_0 . Flexion mode movement at screws fixation angle of $\vec{\alpha} = (-5, 0)$.

previous mesh sensitivity analysis, with a mesh of 200.000 elements, a screws insertion angle of $\vec{\alpha} = (-5, 0)$ in a flexion mode motion, Fig. 5 indicates that the apparent peak load from the phase field scheme increases as the characteristic length scale l_0 is reduced, as expected based on previous results reported in the literature [65, 66].

6. Computational analysis

6.1. Characterization of loading modes

Continuing with the comparative investigation of the various screw insertion angles, namely $\vec{\alpha} = (-5, 0)$, $\vec{\alpha} = (+5, +5)$, and $\vec{\alpha} = (-5, -5)$. Fig. 6 highlights how the screw configuration influences the mechanical responses of the vertebral body in different motion regimes. The Force vs. Displacement curves generated from the phase field finite element method are displayed in Figs. 6(a), 6(c), and 6(e), representing the vertebral movements of flexion, extension, and torsion, respectively.

In the three cases analyzed, the Load is computed as the vincular reaction on the bottom of the vertebra. In the cases of flexion and extension there is a linear elastic phase, followed by a softening due to the occurrence of fracture inside the vertebra, whereas in the case of rotation, the vincular reaction on the bottom is equal to zero, until a critical angle is reached and the fracture is activated.

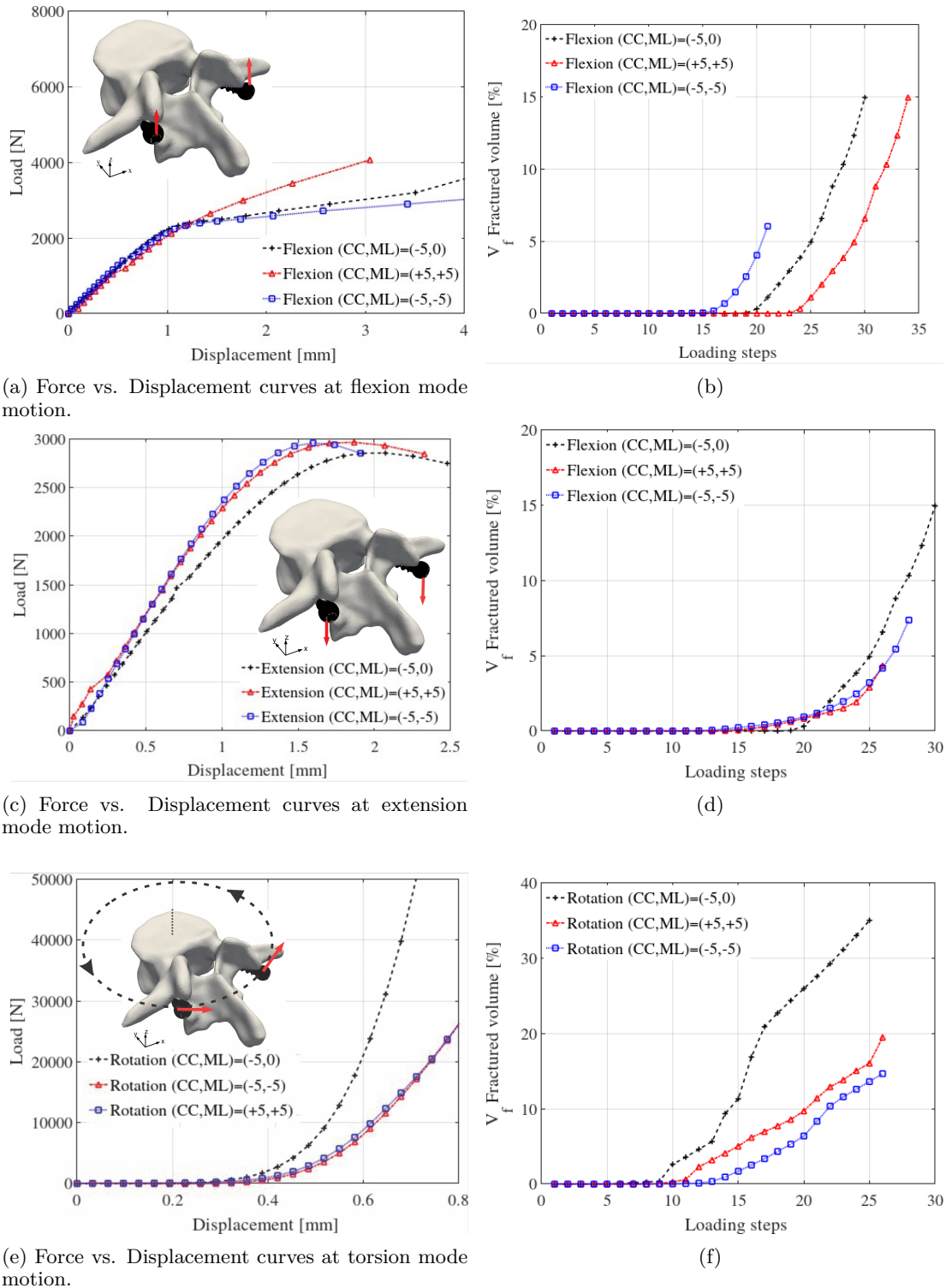
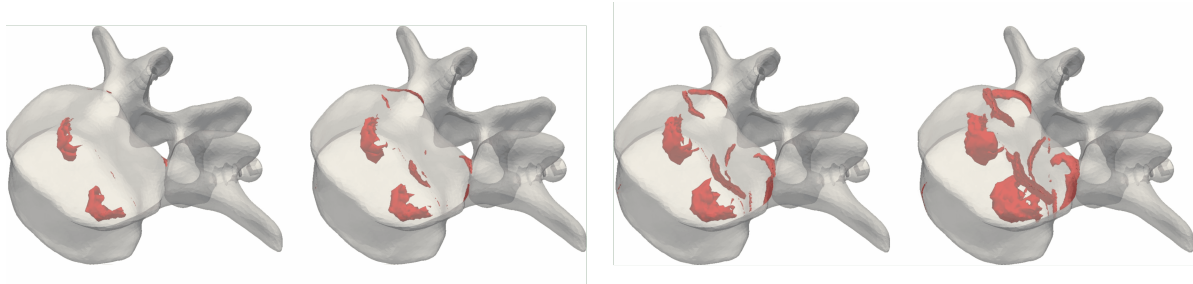


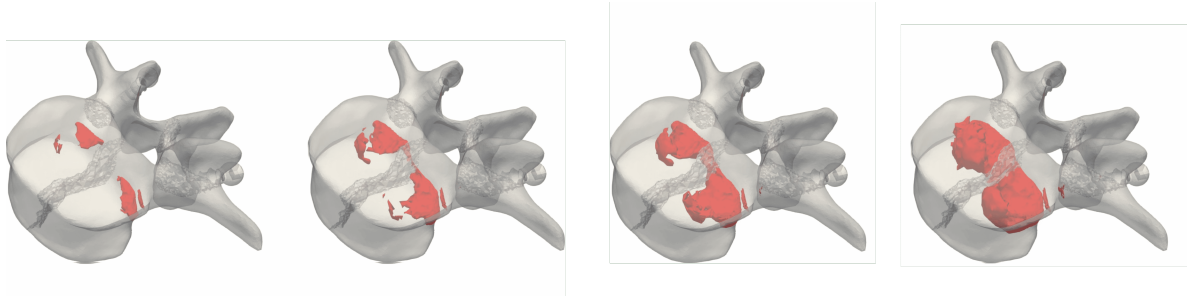
Fig. 6: Comparative analyses among the flexion, extension and torsion modes, at screws fixation angles of $\vec{\alpha} = (-5, 0)$, $\vec{\alpha} = (+5, +5)$ and $\vec{\alpha} = (-5, -5)$.

Regarding the damage patterns, the counter-clockwise torsion motions simulated for

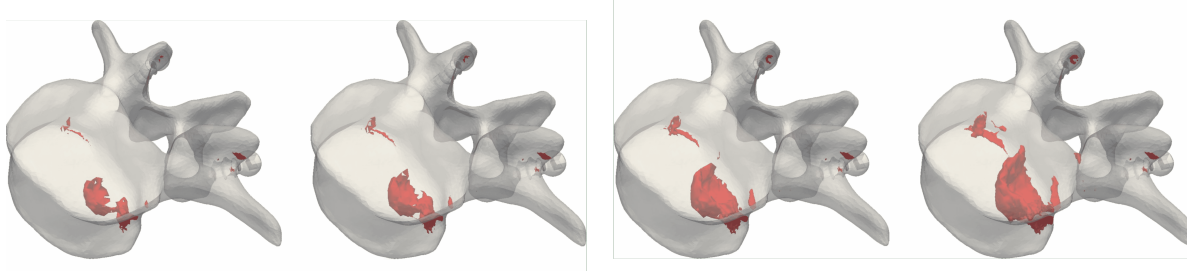
the insertion angles $\vec{\alpha} = (-5, 0)$, $\vec{\alpha} = (+5, +5)$, and $\vec{\alpha} = (-5, -5)$ were characterized by the formation of asymmetric damage, where damage occurrence is more prominent on the side that experiences greater loading as the steps increase. Additionally, in terms of flexion and extension regimes, symmetrical patterns were observed for all three screw fixation angle combinations, as expected. These characterizations further validate the effectiveness of the present phase field modeling as a powerful tool for capturing damage in biological tissues. Moreover, they demonstrate good agreement with recent works found in the literature [25, 29].



(a) Back view of the evolution of the fracture pattern under vertical extension loading.



(b) Back view of the evolution of the fracture pattern under vertical flexion loading regime.



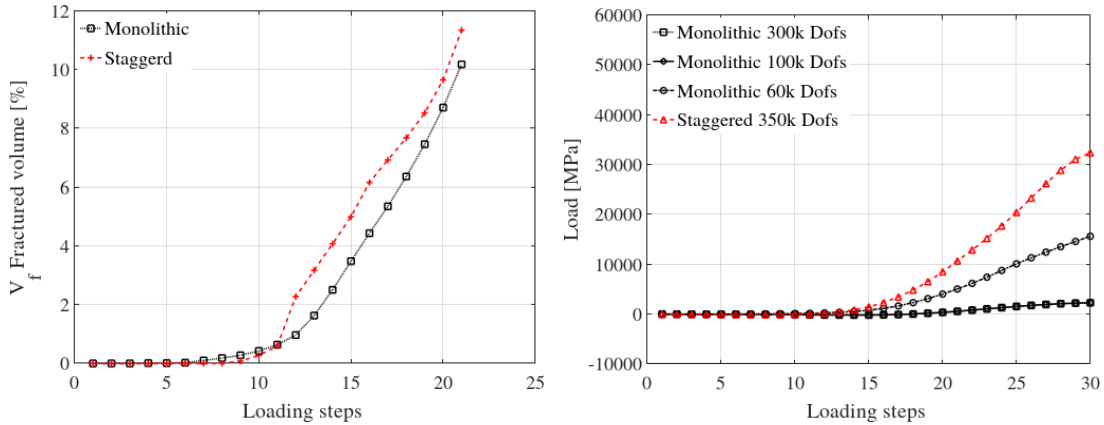
(c) Back view of the evolution of the fracture pattern under a counter-clockwise axial rotation loading regime applied on the head of the screws.

Fig. 7: Evolution of the damage pattern caused by loading regimes applied on the pedicle screws head: (a) extension motion; (b) flexion motion; and (c) counter-clockwise axial rotation motion.

6.2. Staggered vs monolithic numerical schemes

A numerical comparison has been conducted to assess the performances of both the staggered and monolithic numerical schemes, as described in Secs. 4.1 and 4.3, respectively, in terms of their accuracy in reproducing the fracture patterns and the Load vs. Displacement curves.

For this comparative analysis, the discretized vertebra-screws model consisting of 300.000 elements has considered, with the screws inserted at an angle combination of $\vec{\alpha} = (-5, 0)$, in a counter-clockwise torsion motion. It is notable that the fracture pattern obtained from the monolithic method bears resemblance to the damage patterns observed in the staggered simulation, see Fig. 9. Furthermore, the fractioned volume outcomes are similar for both approaches. It can also be observed that, in terms of accuracy, the Load vs Displacement curves are more accurate in the monolithic scheme due to the fact that the binding reaction on the vertebra endplate is zero and deviates very little. Nevertheless, considering the computational time consumed, the advantages of using the staggered scheme outweigh the potential benefits offered by the monolithic technique. While the staggered simulation took approximately 3.5 hours to complete, the monolithic running time exceeded 15 hours.



(a) Applied loading on a counter-clockwise axial rotation loading regime applied on the head of the screws as function of the loading step. (b) Fractured volume of the vertebra on a counter-clockwise axial rotation loading regime applied on the head of the screws as the loading step increases.

Fig. 8: Staggered and monolithic phase field models contrasted on a counter-clockwise axial rotation regime.

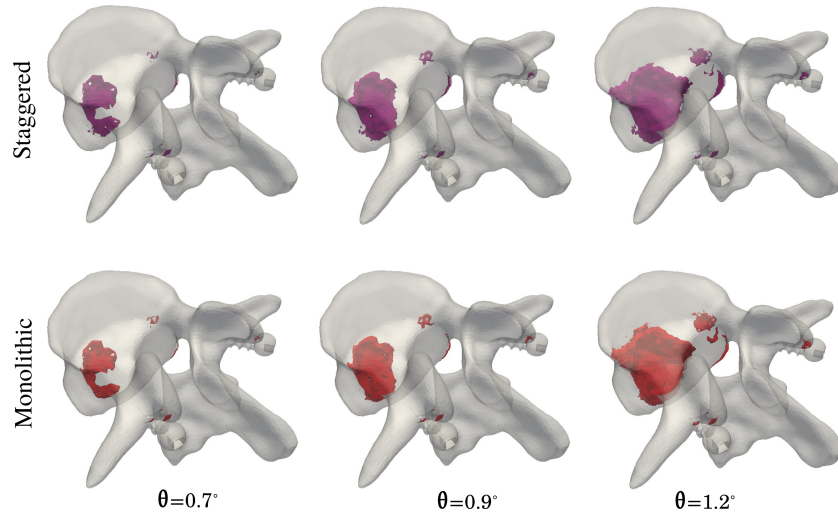


Fig. 9: Damage pattern comparisons between staggered and monolithic phase field models on a counter-clockwise axial rotation regime.

7. Conclusions

A careful assessment of the fracture patterns and associated mechanisms in a human vertebra after the insertion of pedicle screws was scrutinized by implementing a finite element phase field method. Throughout the study, several aspects were pondered to accurately investigate the fractures and crack trajectories, such as maximum yield stress, critical energy release rate, and the characteristic length scale.

The analysis of various fracture types was ensured by conducting a mesh sensitivity study, which provided an optimal mesh size balancing simulation running time and the model's capability to reproduce outcomes within a small relative error. These findings were supported by comparing Force vs. Displacement curves for all considered mesh refinements at the extension vertebral motion mode and a screws insertion angle configuration of $\vec{\alpha} = (-5, 0)$. It is worth mentioning that the damage responses in the vertebra from the developed phase field model are affected when different configurations of the pedicle screws fixation angle are simulated.

In addition, a comparison between phase field finite element approaches was also performed. Essentially, the staggered phase field model makes headway in terms of optimizing computational time consumption in relation to characterizing the damage within the vertebra-screws model, when compared to the results obtained from the monolithic phase field scheme.

References

- [1] Andrea Braides et al. *Approximation of free-discontinuity problems*. Number 1694. Springer Science & Business Media, 1998.
- [2] Andrea Braides. γ -convergence for beginners. *Oxford Lecture Series in Mathematics and its Applications*, 22, 2002.

- [3] Luigi Ambrosio and Vincenzo Maria Tortorelli. Approximation of functional depending on jumps by elliptic functional via Γ -convergence. *Communications on Pure and Applied Mathematics*, 43(8):999–1036, 1990.
- [4] Luigi Ambrosio. On the approximation of free discontinuity problems. *Boll. Un. Mat. Ital., B*, (7):105–123, 1992.
- [5] Gilles A Francfort and J-J Marigo. Revisiting brittle fracture as an energy minimization problem. *Journal of the Mechanics and Physics of Solids*, 46(8):1319–1342, 1998.
- [6] Zdenek P Bazant. Crack band model for fracture of geomaterials. In *Unknown Host Publication Title*, pages 1137–1152. AA Balkema, 1982.
- [7] Zdeněk P Bažant and Feng-Bao Lin. Nonlocal smeared cracking model for concrete fracture. *Journal of structural Engineering*, 114(11):2493–2510, 1988.
- [8] ZP Bazant and M Jirasek. Damage nonlocality due to microcrack interactions: statistical determination of crack influence function. *Fracture and Damage in Quasi-brittle Structures*, pages 3–17, 1994.
- [9] Bruno Gerard, Gilles Pijaudier-Cabot, and Christian Laborderie. Coupled diffusion-damage modelling and the implications on failure due to strain localisation. *International Journal of Solids and Structures*, 35(31-32):4107–4120, 1998.
- [10] MGD Geers, R De Borst, WAM Brekelmans, and RHJ0938 Peerlings. Strain-based transient-gradient damage model for failure analyses. *Computer methods in applied mechanics and engineering*, 160(1-2):133–153, 1998.
- [11] Blaise Bourdin, Gilles A Francfort, and Jean-Jacques Marigo. Numerical experiments in revisited brittle fracture. *Journal of the Mechanics and Physics of Solids*, 48(4):797–826, 2000.
- [12] Blaise Bourdin, Gilles A Francfort, and Jean-Jacques Marigo. The variational approach to fracture. *Journal of elasticity*, 91(1):5–148, 2008.
- [13] Charlotte Kuhn and Ralf Müller. A phase field model for fracture. In *PAMM: Proceedings in Applied Mathematics and Mechanics*, volume 8, pages 10223–10224. Wiley Online Library, 2008.
- [14] Vincent Hakim and Alain Karma. Laws of crack motion and phase-field models of fracture. *Journal of the Mechanics and Physics of Solids*, 57(2):342–368, 2009.
- [15] Hanen Amor, Jean-Jacques Marigo, and Corrado Maurini. Regularized formulation of the variational brittle fracture with unilateral contact: Numerical experiments. *Journal of the Mechanics and Physics of Solids*, 57(8):1209–1229, 2009.

- [16] Thanh Tung Nguyen, Julien Yvonnet, Q-Z Zhu, Michel Bornert, and Camille Chateau. A phase field method to simulate crack nucleation and propagation in strongly heterogeneous materials from direct imaging of their microstructure. *Engineering Fracture Mechanics*, 139:18–39, 2015.
- [17] Mohammed A Msekh, Juan Michael Sargado, Mostafa Jamshidian, Pedro Miguel Areias, and Timon Rabczuk. Abaqus implementation of phase-field model for brittle fracture. *Computational Materials Science*, 96:472–484, 2015.
- [18] Daniel Jodlbauer, Ulrich Langer, and Thomas Wick. Parallel matrix-free higher-order finite element solvers for phase-field fracture problems. *Mathematical and Computational Applications*, 25(3):40, 2020.
- [19] Jian-Ying Wu. A unified phase-field theory for the mechanics of damage and quasi-brittle failure. *Journal of the Mechanics and Physics of Solids*, 103:72–99, 2017.
- [20] Christian Miehe, Martina Hofacker, and Fabian Welschinger. A phase field model for rate-independent crack propagation: Robust algorithmic implementation based on operator splits. *Computer Methods in Applied Mechanics and Engineering*, 199(45-48):2765–2778, 2010.
- [21] Christian Miehe, Fabian Welschinger, and Martina Hofacker. Thermodynamically consistent phase-field models of fracture: Variational principles and multi-field fe implementations. *International journal for numerical methods in engineering*, 83(10):1273–1311, 2010.
- [22] Erwan Tanné, Tianyi Li, Blaise Bourdin, J-J Marigo, and Corrado Maurini. Crack nucleation in variational phase-field models of brittle fracture. *Journal of the Mechanics and Physics of Solids*, 110:80–99, 2018.
- [23] Daniele Bianchi, Cristina Falcinelli, Leonardo Molinari, Alessio Gizzi, and Alberto Di Martino. Osteolytic vs. osteoblastic metastatic lesion: Computational modeling of the mechanical behavior in the human vertebra after screws fixation procedure. *Journal of Clinical Medicine*, 11(10):2850, 2022.
- [24] Anna Gustafsson and Hanna Isaksson. Phase field models of interface failure for bone application-evaluation of open-source implementations. *Theoretical and Applied Fracture Mechanics*, page 103432, 2022.
- [25] Leonardo Molinari, Cristina Falcinelli, Alessio Gizzi, and Alberto Di Martino. Biomechanical modeling of metal screw loadings on the human vertebra. *Acta Mechanica Sinica*, 37(2):307–320, 2021.
- [26] Tetsuro Ohba, Shigeto Ebata, Hiroki Oba, Kensuke Koyama, and Hirotaka Haro. Risk factors for clinically relevant loosening of percutaneous pedicle screws. *Spine Surgery and Related Research*, 3(1):79–85, 2019.

- [27] William Sterba, Do-Gyoon Kim, David P Fyhrie, Yener N Yeni, and Rahul Vaidya. Biomechanical analysis of differing pedicle screw insertion angles. *Clinical biomechanics*, 22(4):385–391, 2007.
- [28] Serkan Inceoğlu, William H Montgomery, Selvon St Clair, and Robert F McLain. Pedicle screw insertion angle and pullout strength: comparison of 2 proposed strategies. *Journal of Neurosurgery: Spine*, 14(5):670–676, 2011.
- [29] Leonardo Molinari, Cristina Falcinelli, Alessio Gizzi, and Alberto Di Martino. Effect of pedicle screw angles on the fracture risk of the human vertebra: a patient-specific computational model. *Journal of the Mechanical Behavior of Biomedical Materials*, 116:104359, 2021.
- [30] Zohar Yosibash, David Tal, and Nir Trabelsi. Predicting the yield of the proximal femur using high-order finite-element analysis with inhomogeneous orthotropic material properties. *Philosophical Transactions of the Royal Society A: Mathematical, Physical and Engineering Sciences*, 368(1920):2707–2723, 2010.
- [31] Y Matsuura, H Giambini, Y Ogawa, Z Fang, AR Thoreson, MJ Yaszemski, L Lu, and KN An. Specimen-specific nonlinear finite element modeling to predict vertebrae fracture loads after vertebroplasty. *Spine*, 39(22):E1291, 2014.
- [32] Martin Sandve Alnæs, Johan Hake, Robert C Kirby, Hans Petter Langtangen, Anders Logg, and Garth N Wells. The fenics manual. *FEniCS Project, version October 31st*, 36, 2011.
- [33] Rahul Pongiman. *HyperMesh Introduction Pre-Processing for Finite Element Analysis*. Altair University, 2014.
- [34] Christophe Geuzaine and Jean-François Remacle. Gmsh: A 3-d finite element mesh generator with built-in pre-and post-processing facilities. *International journal for numerical methods in engineering*, 79(11):1309–1331, 2009.
- [35] Ravi K Nalla, Jamie J Kruzic, John H Kinney, and Robert O Ritchie. Effect of aging on the toughness of human cortical bone: evaluation by r-curves. *Bone*, 35(6):1240–1246, 2004.
- [36] Aaron J Fields, Gideon L Lee, and Tony M Keaveny. Mechanisms of initial endplate failure in the human vertebral body. *Journal of biomechanics*, 43(16):3126–3131, 2010.
- [37] Ibrahim Erdem, Eeric Truumees, and Marjolein CH van der Meulen. Simulation of the behaviour of the l1 vertebra for different material properties and loading conditions. *Computer methods in biomechanics and biomedical engineering*, 16(7):736–746, 2013.

- [38] Liwen Lin, Hui Wang, Ming Ni, Yunfeng Rui, Tian-Yuan Cheng, Cheng-Kung Cheng, Xiaohua Pan, Gang Li, and Changjian Lin. Enhanced osteointegration of medical titanium implant with surface modifications in micro/nanoscale structures. *Journal of Orthopaedic Translation*, 2(1):35–42, 2014.
- [39] Kaile Song, Zhaohui Wang, Jing Lan, and Songhua Ma. Porous structure design and mechanical behavior analysis based on tpms for customized root analogue implant. *Journal of the Mechanical Behavior of Biomedical Materials*, 115:104222, 2021.
- [40] AN Aufa, Mohamad Zaki Hassan, and Zarini Ismail. Recent advances in ti-6al-4v additively manufactured by selective laser melting for biomedical implants: Prospect development. *Journal of Alloys and Compounds*, 896:163072, 2022.
- [41] Alan Arnold Griffith. Vi. the phenomena of rupture and flow in solids. *Philosophical transactions of the royal society of london. Series A, containing papers of a mathematical or physical character*, 221(582-593):163–198, 1921.
- [42] Gianpietro Del Piero, Giovanni Lancioni, and Riccardo March. A variational model for fracture mechanics: numerical experiments. *Journal of the Mechanics and Physics of Solids*, 55(12):2513–2537, 2007.
- [43] Marino Arroyo and Michael Ortiz. Local maximum-entropy approximation schemes: a seamless bridge between finite elements and meshfree methods. *International journal for numerical methods in engineering*, 65(13):2167–2202, 2006.
- [44] M Hofacker and C30082661352 Miehe. A phase field model of dynamic fracture: Robust field updates for the analysis of complex crack patterns. *International Journal for Numerical Methods in Engineering*, 93(3):276–301, 2013.
- [45] Christian Miehe, Lisa-Marie Schaezel, and Heike Ulmer. Phase field modeling of fracture in multi-physics problems. part i. balance of crack surface and failure criteria for brittle crack propagation in thermo-elastic solids. *Computer Methods in Applied Mechanics and Engineering*, 294:449–485, 2015.
- [46] Christian Miehe, M Hofacker, L-M Schänzel, and Fadi Aldakheel. Phase field modeling of fracture in multi-physics problems. part ii. coupled brittle-to-ductile failure criteria and crack propagation in thermo-elastic–plastic solids. *Computer Methods in Applied Mechanics and Engineering*, 294:486–522, 2015.
- [47] Thanh-Tung Nguyen, Julien Yvonnet, Q-Z Zhu, Michel Bornert, and Camille Chateau. A phase-field method for computational modeling of interfacial damage interacting with crack propagation in realistic microstructures obtained by microtomography. *Computer Methods in Applied Mechanics and Engineering*, 312:567–595, 2016.

- [48] Bernard D Coleman and Walter Noll. The thermodynamics of elastic materials with heat conduction and viscosity. In *The Foundations of Mechanics and Thermodynamics*, pages 145–156. Springer, 1974.
- [49] Jef Wambacq, Jacinto Ulloa, Geert Lombaert, and Stijn François. Interior-point methods for the phase-field approach to brittle and ductile fracture. *Computer Methods in Applied Mechanics and Engineering*, 375:113612, 2021.
- [50] Marreddy Ambati, Tymofiy Gerasimov, and Laura De Lorenzis. A review on phase-field models of brittle fracture and a new fast hybrid formulation. *Computational Mechanics*, 55:383–405, 2015.
- [51] Kim Pham, Hanen Amor, Jean-Jacques Marigo, and Corrado Maurini. Gradient damage models and their use to approximate brittle fracture. *International Journal of Damage Mechanics*, 20(4):618–652, 2011.
- [52] Emilio Martínez-Pañeda, Alireza Golahmar, and Christian F Niordson. A phase field formulation for hydrogen assisted cracking. *Computer Methods in Applied Mechanics and Engineering*, 342:742–761, 2018.
- [53] Deison Prêve, Pietro Lenarda, Ian Maskey, and Marco Paggi. A comprehensive characterization of fracture in unit cell open foams generated from triply periodic minimal surfaces. *Engineering Fracture Mechanics*, .:108949, 2022.
- [54] Tony S Keller. Predicting the compressive mechanical behavior of bone. *Journal of biomechanics*, 27(9):1159–1168, 1994.
- [55] JH Keyak, IY Lee, and HB Skinner. Correlations between orthogonal mechanical properties and density of trabecular bone: use of different densitometric measures. *Journal of biomedical materials research*, 28(11):1329–1336, 1994.
- [56] Philippe K Zysset, X Edward Guo, C Edward Hoffer, Kristin E Moore, and Steven A Goldstein. Elastic modulus and hardness of cortical and trabecular bone lamellae measured by nanoindentation in the human femur. *Journal of biomechanics*, 32(10):1005–1012, 1999.
- [57] Anna Gustafsson, Mathias Wallin, and Hanna Isaksson. Age-related properties at the microscale affect crack propagation in cortical bone. *Journal of biomechanics*, 95:109326, 2019.
- [58] Anna Gustafsson, Mathias Wallin, Hanifeh Khayyeri, and Hanna Isaksson. Crack propagation in cortical bone is affected by the characteristics of the cement line: a parameter study using an xfm interface damage model. *Biomechanics and modeling in mechanobiology*, 18(4):1247–1261, 2019.
- [59] Kwai S Chan, Candace K Chan, and Daniel P Nicolella. Relating crack-tip deformation to mineralization and fracture resistance in human femur cortical bone. *Bone*, 45(3):427–434, 2009.

- [60] KJ Koester, HD Barth, and RO Ritchie. Effect of aging on the transverse toughness of human cortical bone: evaluation by r-curves. *Journal of the mechanical behavior of biomedical materials*, 4(7):1504–1513, 2011.
- [61] Rilin Shen, Haim Waisman, Zohar Yosibash, and Gal Dahan. A novel phase field method for modeling the fracture of long bones. *International Journal for Numerical Methods in Biomedical Engineering*, 35(8):e3211, 2019.
- [62] L Hug, G Dahan, S Kollmannsberger, E Rank, and Z Yosibash. Predicting fracture in the proximal humerus using phase field models. *Journal of the Mechanical Behavior of Biomedical Materials*, 134:105415, 2022.
- [63] M Dreischarf, T Zander, A Shirazi-Adl, CM Puttlitz, CJ Adam, CS Chen, VK Goel, A Kiapour, YH Kim, KM Labus, et al. Comparison of eight published static finite element models of the intact lumbar spine: predictive power of models improves when combined together. *Journal of biomechanics*, 47(8):1757–1766, 2014.
- [64] Keitaro Matsukawa, Yoshiyuki Yato, Hideaki Imabayashi, Naobumi Hosogane, Takashi Asazuma, and Koichi Nemoto. Biomechanical evaluation of the fixation strength of lumbar pedicle screws using cortical bone trajectory: a finite element study. *Journal of Neurosurgery: Spine*, 23(4):471–478, 2015.
- [65] Marco Paggi and José Reinoso. Revisiting the problem of a crack impinging on an interface: a modeling framework for the interaction between the phase field approach for brittle fracture and the interface cohesive zone model. *Computer Methods in Applied Mechanics and Engineering*, 321:145–172, 2017.
- [66] PK Asur Vijaya Kumar, A Dean, J Reinoso, P Lenarda, and M Paggi. Phase field modeling of fracture in functionally graded materials: γ -convergence and mechanical insight on the effect of grading. *Thin-Walled Structures*, 159:107234, 2021.